On the Broadening of the Characteristic Frequency Range towards Higher Photon Energies in the X-ray Variability of the Black Hole Transient MAXI J1820+070

CHENXU GAO D, 1,2 WENFEI YU D, 1 AND ZHEN YAN D1

¹Shanghai Astronomical Observatory, Chinese Academy of Sciences,
 80 Nandan Road, Shanghai 200030, China
 ²University of Chinese Academy of Sciences, 19A Yuquan Road, Beijing 100049, China

ABSTRACT

Energy-dependence of X-ray Fourier power spectral states and the characteristic frequencies of the Band-Limited Noise (BLN) components have been seen in the hard state and intermediate states of black hole X-ray binaries. Here we report our analysis of the Insight-HXMT observations of the black hole transient MAXI J1820+070 during its 2018 outburst when the source was brightest in hard X-rays. We found opposite trends of the low-frequency (< 0.1 Hz) and the high-frequency (>10 Hz) BLN components, i.e., decreasing vs. increasing in frequency with increasing photon energy up to beyond 200 keV, respectively. This establishes an apparent two-way broadening of the power plateau formed by multiple BLNs in the power spectra towards higher photon energies. The trend of increasing characteristic frequency of the highest BLN component with increasing photon energy has been interpreted as due to that the corresponding seed photons which are up-scatted to relatively higher energies originate in a region relatively more central in the corona previously. Following the same framework, the decreasing trend of the characteristic frequency of the low-frequency BLN component with increasing photon energy can be interpreted as due to that the corresponding seed photons which are up-scattered to higher photon energies originate from further out in the disk flow but on the opposite side of the central corona as to the observer. The opposite trends then implies that the the plateau in the power spectra formed by the multiple BLNs represents the radial extension of the accretion disk that contributes seed photons which produce the observed BLNs; the higher the photon energy is, the wider the power plateau and the smaller the fractional variability are, probably approaching to a Power-Law Noise (PLN) seen in the soft state.

Keywords: accretion, accretion discs – stars: black holes – X-rays: binaries – X-rays: individual: MAXI J1820+070

1. INTRODUCTION

Most known black hole X-ray binaries (BH XRBs) in our galaxy are transient low-mass X-ray binary (LMXB) sources. They spent most of their time in quiescence and occasionally turned into an accretion outburst. During such an outburst, the corresponding X-ray spectral and timing properties usually evolve on timescales from days to months (see reviews by Remillard & McClintock 2006; Done et al. 2007; Belloni & Motta 2016). Different X-ray spectral states are classified on the basis of the X-ray spectral and timing properties seen with X-ray observations (Homan et al. 2001). The two main spectral states are the low-hard state (LHS) and high-soft state (HSS) which have been identified (Tananbaum et al. 1972).

X-ray variability in black hole X-ray binaries has been detected in a wide range of time scales during X-ray binary outbursts when the X-ray intensity is high enough, whereas the shortest time scales of the variability in the X-ray band is comparable to the dynamical time scales around the compact objects(Van der Klis 2006). The conventional way

Corresponding author: Wenfei Yu

wenfei@shao.ac.cn

for examining such variability components within the realm of BHXB fluctuations is the analysis through the Power Density Spectrum (PDS), enabling the investigation of both quasi-periodic oscillations (QPOs) and broadband noise in the Fourier frequency domain. The power spectrum in black hole HSS is characterized primarily by a Power-law Noise (PLN), while the power spectrum in black hole LHS is primarily dominated by one or more Band-Limited Noise (BLN) components with additional QPOs. The power spectrum corresponding to the intermediate BH state consists of BLN and QPO, but sometimes there is also a weak PLN component(Belloni et al. 2002).

The popular picture of the correlated spectral and temporal states is significantly challenged by the observations of the black hole X-ray binary candidate MAXI J1659-152 (Yu & Zhang 2013). In that study, the authors have identified pronounced energy-dependence in its PDS characteristics. Specifically, during the transition from the hard to intermediate states, the PDS of the soft X-ray energy band below 2 keV, which corresponds to the disk spectral component, exhibited characteristics typical of the HSS by showing a PLN, while the hard X-ray energy band (> 2 keV), corresponding to the Comptonized component, exhibited characteristics of the LHS by showing BLNs and QPO. This demonstrates that black hole power spectral states actually depend on which spectral components we are looking at. In other words, there is no actual correspondence between the energy spectral state and the power spectral state. Moreover, subsequent studies on the energy dependence of the PDS of GRS 1915+105 yielded similar findings (Stiele & Yu 2014). This further suggests that timing analysis in the soft X-ray energy band (< 2 keV) is more sensitive to trace the emergence of the thermal disk component compared to spectral analysis.

Through power spectral analysis of various types of X-ray binaries, Wijnands & Klis (1999) discovered a strong correlation between the QPO frequency (the low-frequency QPO) and the break frequency of BLN. This suggests that BLN and QPO may originate from the same physical mechanism or somehow couple under a certain unknown mechanism. On the other hand, Yu et al. (2003) show that the spectral transitions in the neutron star LMXB transient Aquila X-1 share a great similarity to those of black hole transients. Specifically, they show the primary BLN and the low frequency QPO in both black hole and neutron star systems follow an identical correlation between the break frequency of the BLN and the frequency of the low frequency QPO. This demonstrate that the BLN and the QPO in BH X-ray binaries are of the same origins as those of the neutron star systems Yu et al. (2003). Correlation between the kHz QPO frequency and the X-ray count rate on the BLN time scales in the Z type neutron star LMXB Sco X-1 have demonstrated that the BLN corresponds to the modulation in the mass accretion rate. In addition, in the atoll type neutron star low-mass X-ray binaries, the frequencies of the kilohertz QPOs correlate with X-ray intensity on time scales from seconds to a few tens of seconds, i.e., the BLN time scales, in observations of hours and establish the so-called 'parallel track' phenomenon (Yu et al. 1997; Méndez et al. 1999). This also implies that the BLN corresponds to the variation in the mass accretion rate. In fact, modeling of the X-ray variability of the accretion flow based on the propagation scenario (Lyubarskii 1997) has reproduced the BLN components in the PDS (Ingram & Done 2011).

Stiele & Yu (2014) has detected the energy dependence of the characteristic frequency of the BLN in 1H 1743-322 for the first time in a black hole transient, strengthening the energy-dependent picture of the power spectra of black hole X-ray binaries (Yu & Zhang 2013). The characteristic frequency of the BLN increased with increasing photon energy in the energy range below 10 keV as seen with the XMM-Newton. Yang et al. (2022) show the same energy dependence of the characteristic frequency of the BLN extends to the hard X-ray band in MAXI J1820+070, beyond a few tens of keV. In Gao et al. (2023), we analyzed the modulation of spectral components in different phases of the LFQPO during a hard-state observation of MAXI J1820+070. We suggested that the original beats of the LFQPO come from the Compton component. In the above analysis, we detected the energy-dependence of the BLN at the highest frequency in MAXI J1820+070 with *Insight*-HXMT that was reported in Yang et al. (2022), but with additional new discoveries regarding the behaviour of the BLN component at the low frequency end. Here we present our findings of the energy dependence of the BLNs with the *Insight*-HXMT observations.

2. OBSERVATIONS AND DATA REDUCTION

The black hole transient MAXI J1820+070 was first discovered in X-ray emissions on 11 March 2018, by the Monitor of All-sky X-ray Image (MAXI; Kawamuro et al. 2018; Tucker et al. 2018). During the onset of the outburst, its luminosity exhibited a rapid rise, reaching a level of 2 Crab within the energy range of 2-20 keV (Shidatsu et al. 2018). Subsequently, the source sustained a prolonged period of approximately three months in the black hole hard state, characterized by a slight decline in luminosity (Shidatsu et al. 2019). The long-lived hard state provides an exceptional opportunity to investigate its X-ray timing and spectral behavior (e.g. Buisson et al. 2019; Kara et al. 2019), especially in the hard X-ray energies with *Insight*-HXMT (Ma et al. 2020). NICER and *Insight*-HXMT observations of MAXI

J1820+070 (Kawamura et al. 2022; Yang et al. 2022) have shown the energy dependence of the characteristic frequency of the BLN at the highest frequency, confirming the energy dependence of the BLN in BH XRBs found previously Stiele & Yu (2014).

2.1. Observations

Insight-HXMT consists of three payloads: high-energy X-ray telescope (HE, 35-250 keV), medium-energy X-ray telescope (ME, 10-35 keV), and low-energy X-ray telescope (LE, 1-10 keV)(Zhang et al. 2020). The technical details of Insight-HXMT can be seen in the data reduction guide¹. In our analysis, we utilized the HXMT Data Analysis Software (HXMTDAS) version 2.05, specifically designed for Insight-HXMT data processing. To ensure minimized influence from neighboring sources, we opted for narrow field of views (FOVs) for all three telescopes. Furthermore, we followed the recommended criteria outlined in the guide for producing accurate and reliable Good-Time Intervals (GTIs).

2.2. Data reduction

In the analysis, we computed the Miyamoto normalized PDS for photon series in different energy bands. For data obtained with the LE and ME instruments, we utilized a time interval of 512 seconds and a time resolution of 1/512 seconds, resulting in a Nyquist frequency of 256 Hz. For data obtained with the HE instruments, we employed a time interval of 512 seconds and a time resolution of 1/2048 seconds, corresponding to a Nyquist frequency of 1048 Hz.

For the PDS corresponding to the LE and ME instruments, we calculated the average power above 64 Hz in the PDS and took it as the white noise level. For the HE instrument, we specifically generated the PDS of the photon series obtained with the blocked collimator to ensure an accurate determination of the white noise level, free from potential background model biases. We then calculated the average power above 64 Hz in this PDS, which was taken as the white noise level for the PDS in the HE instrument.

3. POWER SPECTRAL ANALYSIS AND RESULTS

We analyzed only several observations with long exposure times, highest count rates, and notable QPO levels among the HXMT observations (ObsId P011466100601, P011466100701, P011466100801). The PDS was extracted for nine different energy bands: LE (1-2 keV, 2-5 keV, 5-10 keV), ME (10-16 keV, 16-35 keV) and HE (35-46 keV, 46-60 keV, 60-76 keV, 76-100 keV, 100-250 keV). The power spectra were rebinned for analysis focusing on the BLNs. Since these observations were conducted during the hard state of the outburst, we chose to use three or more Lorentzians to model both the QPO and the BLN in each energy band. The PDS fitting procedure was performed using XSPEC version 12.11.1. In the QPO fitting, we considered both the harmonic and sub-harmonic frequencies. To model the BLNs, we utilized three zero-centered Lorentzians, representing the three BLN components shown in Figure 1: low-frequency component(L_l), medium-frequency component(L_m), and high-frequency component(L_h). Specifically, we present the results of observation P011466100601, referred to as Obs-0601, as the main representative example in this analysis. Additionally, we reference the stacked dataset of observations P011466100701 and P011466100801, denoted as Obs-0708S, to corroborate and emphasize the findings from Obs-0601. This complementary dataset allows us to validate our primary findings and explore consistencies across similar observational datasets.

In the best-fitting results (with detail shown in Table 1 for obs-0601), we show the characteristic frequencies and fractional root mean square (rms) values. Characteristic frequencies were taken as $\nu_{\text{max}} = \sqrt{\nu_0^2 + (\omega/2)^2}$, where ν_0 represents the centroid frequency and ω denotes the full width at half maximum (FWHM) of the Lorentzian. We use ν_l , ν_m , and ν_h to represent the characteristic frequencies of L_l , L_m , and L_h , respectively. Additionally, ν_{QPO} represents the frequency of the QPO. In Figure 2, we present the power spectra illustrating the data and the best-fitted model for different energy bands of the PDS from Obs-0601. Interestingly, it is evident that as the energy band increases, the two prominent BLN components in the PDS display distinct shifts toward lower and higher frequencies, respectively. To show the energy dependence of PDS more clearly, we carefully divided the HE energy bands. We extracted 11 additional PDS from HE with overlapping energy bands: 40-51keV, 45-56 keV, 50-62keV, 55-69keV, 60-78keV, 65-86keV, 70-93keV, 75-110keV, 80-130keV, 85-150keV, 90-200keV. Figure 3 shows the three frequencies of the center of broadband noise for all energy bands extracted from Obs-0601 with the same colors as highlighted in Figure 1. Similarly, Figure 4 presents the results for the stacked observations of Obs-0708S.

¹ http://hxmten.ihep.ac.cn/SoftDoc/501.jhtml

Table 1. Energy dependence of the characteristic frequency (ν_{max}) and the fractional rms for BLN, supplemented by Pearson correlation coefficients between the linear and photon energies, calculated for all energy bands and for energy levels above 30 keV.

Energy band	L_l		L_m		L_h	
	$ u_{ m max}$	rms	$ u_{ m max}$	${ m rms}$	$ u_{ m max}$	rms
(1)	(2)	(3)	(4)	(5)	(6)	(7)
1-2keV(LE)	$0.12^{+0.02}_{-0.01}$	$0.24^{+0.01}_{-0.01}$	$1.67^{+0.11}_{-0.59}$	$0.01^{+0.01}_{-0.01}$	$1.81^{+0.14}_{-0.14}$	$0.21^{+0.01}_{-0.01}$
2-5keV(LE)	$0.17^{+0.03}_{-0.02}$	$0.24^{+0.01}_{-0.01}$	$2.50^{+0.02}_{-0.83}$	$0.02^{+0.00}_{-0.00}$	$2.79^{+0.22}_{-0.17}$	$0.24^{+0.01}_{-0.01}$
5-10keV(LE)	$0.20^{+0.04}_{-0.03}$	$0.23^{+0.01}_{-0.01}$	$1.81^{+0.74}_{-0.79}$	$0.07^{+0.00}_{-0.00}$	$3.08^{+0.51}_{-0.36}$	$0.24^{+0.01}_{-0.01}$
10-16keV(ME)	$0.11^{+0.02}_{-0.01}$	$0.21^{+0.01}_{-0.01}$	$2.21^{+0.64}_{-0.40}$	$0.15^{+0.00}_{-0.00}$	$5.43^{+0.64}_{-1.43}$	$0.14^{+0.02}_{-0.02}$
16-35 keV(ME)	$0.11^{+0.01}_{-0.01}$	$0.18^{+0.01}_{-0.01}$	$1.49^{+0.53}_{-0.38}$	$0.11^{+0.00}_{-0.00}$	$5.06^{+0.62}_{-0.87}$	$0.15^{+0.01}_{-0.01}$
35-46keV(HE)	$0.11^{+0.01}_{-0.01}$	$0.18^{+0.01}_{-0.01}$	$1.73^{+0.29}_{-0.28}$	$0.14^{+0.00}_{-0.00}$	$6.08^{+0.91}_{-0.79}$	$0.15^{+0.01}_{-0.01}$
46-60keV(HE)	$0.10^{+0.02}_{-0.01}$	$0.15^{+0.01}_{-0.01}$	$1.69^{+0.27}_{-0.49}$	$0.13^{+0.00}_{-0.02}$	$6.55^{+1.14}_{-1.79}$	$0.13^{+0.02}_{-0.00}$
60-76keV(HE)	$0.07^{+0.01}_{-0.01}$	$0.14^{+0.01}_{-0.01}$	$1.33^{+0.39}_{-0.32}$	$0.11^{+0.00}_{-0.00}$	$5.70^{+0.06}_{-1.20}$	$0.14^{+0.01}_{-0.01}$
76-100 keV(HE)	$0.05^{+0.01}_{-0.01}$	$0.13^{+0.01}_{-0.01}$	$1.02^{+0.05}_{-0.42}$	$0.11^{+0.00}_{-0.00}$	$7.46^{+2.24}_{-2.62}$	$0.15^{+0.01}_{-0.01}$
100-250 keV(HE)	$0.03^{+0.01}_{-0.00}$	$0.10^{+0.01}_{-0.01}$	$2.16^{+0.61}_{-0.52}$	$0.11^{+0.00}_{-0.00}$	$11.93^{+6.58}_{-4.62}$	$0.10^{+0.02}_{-0.02}$
Pearson Linear	-0.94	-	0.53	_	0.90	-
Pearson Linear (¿30keV)	-0.89	_	-0.06	_	0.79	_

Note—The main table presents characteristic frequency $\nu_{\rm max}$ and fractional rms values, including 90% confidence intervals.

3.1. Properties of low-frequency component L_l

Among the three zero-centered Lorentzian components describing the power spectrum, L_l has the lowest characteristic frequency (see Table 1 and Figure 3), which is around 0.1 Hz in the X-ray energy band below 30 keV. ν_l does not show a significant trend of change within the X-ray energy band below 30 keV, consistent across the Obs-0708S(see Figure 4). Across all energy bands, the QPO frequency does not change and is around 0.044Hz. The ν_l in the X-ray energy band below 30 keV is slightly more than double the QPO frequency, close to twice the QPO frequency. Starting from 30 keV, ν_l begin to decrease with energy. Between 60 keV and 70 keV, ν_l drops approximately double $\nu_{\rm QPO}$, and from 90 keV onward, it becomes closer to $\nu_{\rm QPO}$. In the energy band above 100 keV, ν_l decreases further to around 0.03 Hz, slightly higher than half $\nu_{\rm QPO}$. This indicates a progressive movement of L_l relative to the QPO as the energy band increases

The rms of the L_l shows a gradual decrease. Specifically, rms remains relatively constant within the energy band covered by LE but starts to decrease gradually from 30 keV onward. In the energy band above 100 keV, the rms is only half of the value observed in the 1-2 keV energy band. This suggests a decreasing amplitude of the L_l as the energy band increases, indicating a change in its strength or contribution to the overall signal.

3.2. Properties of high-frequency component L_h

The L_h has the highest characteristic frequency among the three Lorentz components seen in the power spectra and is always greater than 1 Hz. ν_h began to shift towards higher frequencies starting from the 1-2 keV photon energy band. The ν_h started to rise from around 2 Hz, reaching approximately 5 Hz in about the 30 keV energy band and gone beyond 10 Hz when photon energies went beyond 100 keV.

The rms of L_h is almost identical to that of the L_l ; both did not show significant changes below 10 keV, and started to decrease to about half of their original values at higher photon energies. Furthermore, we plotted the QPO rms in the lower panel of Figure 3, which exhibits a trend very similar to that of ν_h and ν_l . In Gao et al. (2023), we suggest that the monotonic decrease in the trend of QPO rms above 2 keV is due to the modulation of a larger reflective

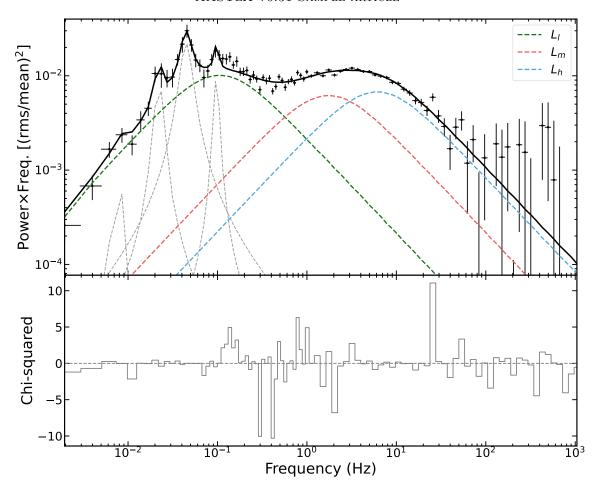


Figure 1. The representative PDS corresponding to the photons in the HE energy range (35-46 keV) of Obs-0601, with the best-fit power spectral models and individual Lorentzian components over-plotted. The light gray dashed line marks the QPO and its harmonic. The dashed lines in green, red, and blue indicate the zero-centered Lorentzian used to describe the BLN components. The bottom panel shows the residuals of the model fit. The plateau of the power spectrum is characterised by the two characteristic frequencies of the low and the high BLN components. i.e., L_l and L_h .

component in the spectral components, with the modulating signal of the reflective component originating from the modulation of the Compton component. Such results demonstrate the intrinsic connection between the QPO and BLN signals in the physical processes.

3.3. Properties of medium-frequency component L_m

The L_m falling between those of L_l and L_h is relatively closer to the latter. In the 1-10 keV energy band, the L_m is almost indistinguishable from L_h at around 2 Hz. However, as the frequency of the ν_h shifts towards higher frequencies, ν_m remained relatively stable in frequency, causing the two noise components to gradually differ towards higher photon energies.

Since L_l and L_h shift towards lower and higher frequencies, respectively, the role of L_m is to represent the flat plateau between the two extreme components. In the 1-10 keV energy band, the L_m has a very small rms ($\lesssim 5\%$). As the photon energy increases, L_m becomes more pronounced. Its rms in the energy band above 35 keV is comparable to that of L_l and L_h .

3.4. Summary

We have investigated the energy-dependence of the BLN components of the X-ray power spectra of the black hole transient MAXI J1820+070 in the energy range of 1-250 keV with HXMT-Insight observations. We found a two-way broadening of the plateau formed by the lowest and highest BLN components in the X-ray power spectra. Specifically,

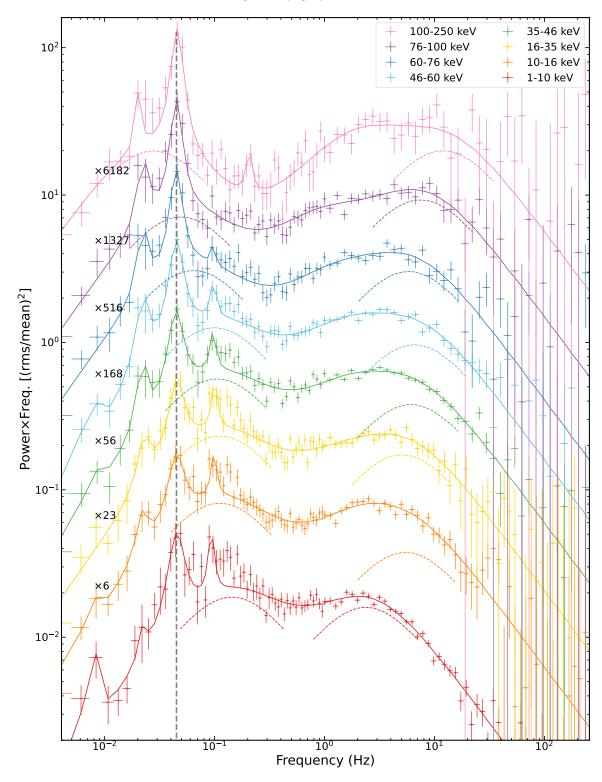


Figure 2. Simultaneous PDS corresponding to photon series in different energy bands obtained from the observation with Obs-0601. The PDS have been shifted vertically to show the trend of the characteristic frequency of the broadband noise in relative photon energy. A vertical grey dashed line marks the frequency of the BH LFQPO. Different colors are used to distinguish the data of different energy bands, with the best-fit models plotted as solid lines. The L_l and L_h are over-plotted to show their opposite trends, establishing a broader plateau of the PDS towards higher photon energies.

the ν_l decreases with increasing photon energy in the energy range above 30 keV; from 0.1 Hz at 1–2 keV to below 0.03 Hz at 100–250 keV. The fractional rms spectrum starts to decrease with increasing energy from 10 keV or so from around 25% at around 1 keV to less than half of it for photon energies above 100 keV. The ν_m remained a rather stable frequency within 1-2 Hz, nearly independent of photon energy. On the other hand, the ν_h increased from about 1 Hz in the 1-2 keV band to about 10 Hz in the energy band beyond 100 keV.

Additionally, we analyzed data from OBS-0708S, which showed results consistent with those from OBS-0601, further validating our observations. This consistency across observations from both OBS-0601 and OBS-0708S underscores the similar patterns of energy dependence exhibited by the BLN components.

We calculated the Pearson correlation coefficients for the characteristic frequencies against photon energies for each BLN component, with detailed results presented in Table 1. Our findings indicate a strong negative correlation between photon energy and the ν_l ; a strong positive correlation for ν_h ; and a weaker correlation for ν_m , revealing significant energy dependence in the BLN and the overall PDS. Additionally, we examined the segments where changes are most pronounced, specifically above 30 keV. We observed that from 30 keV onwards, the correlations between each component and energy show significant changes. Particularly, the correlation for ν_m nearly disappears, while ν_l and ν_h maintain notable correlations, albeit reduced, further validating the presence of energy dependence.

The opposite trends of the evolution of the characteristic frequencies of L_h and L_l with photon energy are visible. To further investigate the trends, we plotted the ratio of the two characteristic frequencies with the change in energy in Figure 5. The results show that the frequency ratio between the L_h and L_l stay under 20 below ~ 20 keV and increases significantly to 400 when the photon energy rose from 10 keV to above 100 keV. The frequency range covered by the BLN components continues to broaden toward both sides with increasing photon energy, showing a wider plateau in the frequency range between 2×10^{-2} Hz and 10 Hz when photon energies are beyond ~ 30 keV.

4. DISCUSSION AND CONCLUSION

The black hole power spectral states have been found dependent on the specific spectral components we are looking at (Yu & Zhang 2013). Specifically, MAXI J1659-152 showed the most extreme transition of the characteristic frequency of the X-ray variability when the photon energy crosses the boundary ~ 2 keV between the disc component and the hard power-law spectral component (Yu & Zhang 2013); the PDS transited from a PLN usually seen in the soft state to a BLN plus QPO type usually seen in hard state or intermediate state. Similar energy dependence of the power spectral states has also been seen in GRS 1915+105 (Stiele & Yu 2014). It is worth noting that a PLN can be interpreted as either the characteristic variability of a BLN evolves to an extremely low or extremely high frequency, or to both. Indeed, the PLN is thought to originate from photons of the X-ray emitting thin disk, from the innermost disk edge to the disk region further out, containing variability in a wider frequency range; the BLN components show variability in a relatively narrow frequency range as compared with the PLN, as those corresponding seed photons are from only the innermost disk subjective to Compton up-scattering by the corona (for example, see the schematic picture discussed in Stiele & Yu (2015)). The above energy dependence of the black hole power spectra reveals clues to the generation of the BLN components as well as providing new clues to the origin of the high-energy photons in black hole binaries through Comptonization.

4.1. Energy-dependent Band-Limited Noise components

Previous studies (Stiele & Yu 2015; Kawamura et al. 2022) of L_h have shown the energy-dependence of the ν_h in BH hard state. Our analysis show the same results as before for the high frequency BLN. But simultaneously with the behaviors of the L_h , we found instead the L_l shifted towards lower frequencies with increasing photon energies. The phenomenon became significant when photon energy goes beyond around 30 keV. It is also worth noting that its characteristic frequency has crossed the frequency of the low-frequency QPOs from above to below with increasing photon energy. In Figure 3, we illustrate the shifts in the characteristic frequency of the L_l component by showing the PDS in different energy bands. The photon energy boundary at ~ 30 keV marks the photon energy beyond which the Compton component dominates. Since BLNs in black hole binaries and neutron star LMXBs are of same origin (Wijnands & Klis 1999; Yu et al. 2003), which likely corresponds to the variation in the mass accretion rate (Yu & Zhang 2013), the variability of the BLN components should come from propagating fluctuations in the accretion disk as proposed (Lyubarskii 1997) or modeled (Ingram & Done 2011).

In our previous spectral analysis (Gao et al. 2023), we found that the broadband X-ray spectrum can be described by a thermal disc component plus a Comptonization component involving disk reflection, in which the disc component

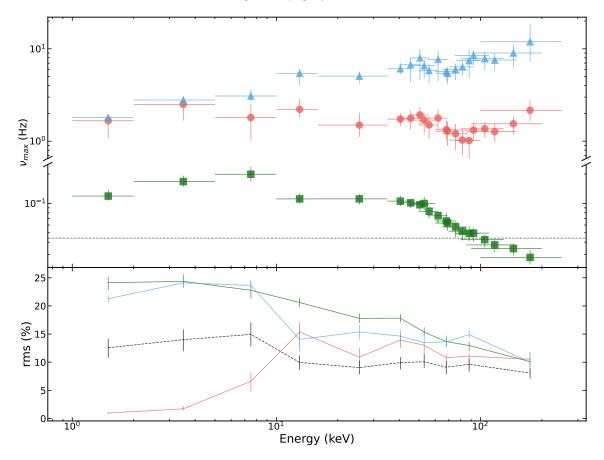


Figure 3. The energy dependence of the characteristic frequency and the fractional rms for the three BLN Lorentzian components. The color scheme of three BLN follows those highlighted in Figure 1. The $\nu_{\rm QPO}$ is indicated by a horizontal dashed line in gray in the upper panel and its fraction rms is represented by gray dashed line in lower panel. A break in the y-axis was implemented to show the trends. Data were extracted from Obs-0601.

provides the seed photons for Comptonization. The results indicate that in the soft X-ray band ($< 10 \,\mathrm{keV}$), the majority of the observed photons originate from the reflection component resulting from the reprocessing of Comptonized photons by the accretion disk and direct disk photons are minimal. In the high-energy hard X-ray band ($> 70 \,\mathrm{keV}$), the spectrum is dominated by the Compton component alone. This suggests that the seed photons responsible for the $> 30 \,\mathrm{keV}$ high energy Compton photons of the BLN at the lowest characteristic frequency originate from the accretion disk further out than those seed photons responsible for those $< 30 \,\mathrm{keV}$ BLN photons in the processes of Comptonization and/or reflection. This also suggests that the X-ray photons producing the broadening of the characteristic frequencies of the BLNs were subjective to the origin of the seed photons in the Comptonization process.

4.2. Possible interpretations

The energy dependence of the characteristic frequencies of the BLNs show opposite trends for the L_l and the L_h , showing a broadening of the plateau between 0.1 Hz and 10 Hz in the PDS towards higher photon energies (see Figure 2) can be explained by extension of the seed photons originated from the accretion disk. Seed photons which carry variability of a certain characteristic frequency in the accretion disk will undergo a number of Compton upscatterings on their ways before they escape the corona and eventually reaches the observer. The exact number of scatterings would be determined by their paths in relative to the corona before going along the observer's line of sight. Our previous spectral investigations show that the average optical depth was around 4.4 (Gao et al. 2023). Early studies of Comptonization and the angular distribution of seed photons, Pozdnyakov et al. (1983) have shown that Comptonized photons with an optical depth exceeding four are nearly entirely emitted along the directions of the incident photons to the corona. Thus the seed photons originating from the very innermost accretion disk can

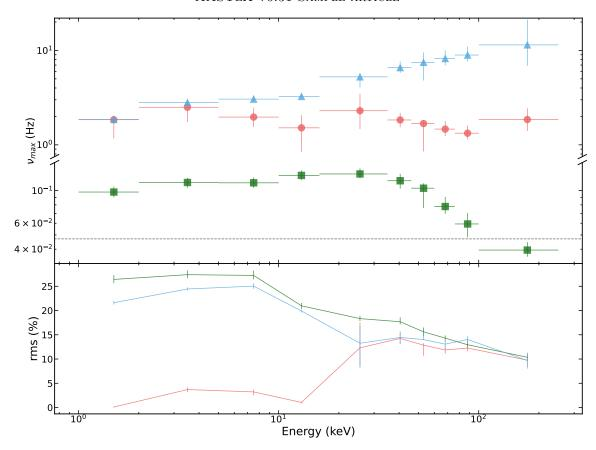


Figure 4. The energy dependence of the characteristic frequencies and fractional rms for the three BLN Lorentzian components is shown, with the colors corresponding to those highlighted in Figure 1. The $\nu_{\rm QPO}$ is indicated by a horizontal dashed line in gray. Data in the plot were derived from the average PDS of the stacked observations Obs-0708S.

go through the corona and reach higher photon energies, generating the BLN component at the highest frequency, as suggested by Stiele & Yu (2015) to explain the energy-dependence of the high frequency BLN.

Stiele & Yu (2015) conducted spectral analysis of PDS for several black hole X-ray binaries. They found that, in the PDS described by BLN and QPO in the hard state, the characteristic frequency of the same BLN component in a harder X-ray band is higher than that in the softer X-ray band with XMM-Newton observations. They interpreted the phenomenon as that the time scales of the seed photons eventually up-scattered to higher energies are shorter because they originate from locations in the disk flow closer to the central black hole. This means that although photons in the soft and hard energy bands contribute to the same BLN component, up-scattered photons with soft energies originate from seed photons originated from the accretion disk at larger radii, hence carry variability at lower characteristic frequencies. This explains the trend of increasing characteristic frequency with increase in photon energy of the highest BLN as seen with HXMT observations up to beyond 100 keV straightforwardly.

On the other hand, seed photons originated from the part of the accretion disk that is on the opposite side but not penetrates into the central corona can still go through the central corona, get up-scattered to high energies, and eventually run into the trajectory to the line of sight of the observer. Since these photons originate from the accretion disk further out, they only carry variability at a lower frequency and therefore can only contribute to produce the low frequency BLN. The schematic picture about the origins of the low frequency BLN and the high frequency BLN in relation to the origins of those seed photons are shown in Figure 6. To consistently explain the energy-dependent behaviours of the multiple BLNs and the energy-dependent broadening of the plateau formed by the BLNs in the PDS, we only need to acknowledge an extended disk region for providing the seed photons for up-scattering. Extending to higher photon energies, the plateau in the PDS is expected to be more broad and flat. The ultimate limits on such a broadening in terms of characteristic frequencies and total fractional rms might be set by the PLN seen in BH soft state (see Figure 6), as the PLN is formed from the thermal emission of an entire optically-thick accretion disk. In

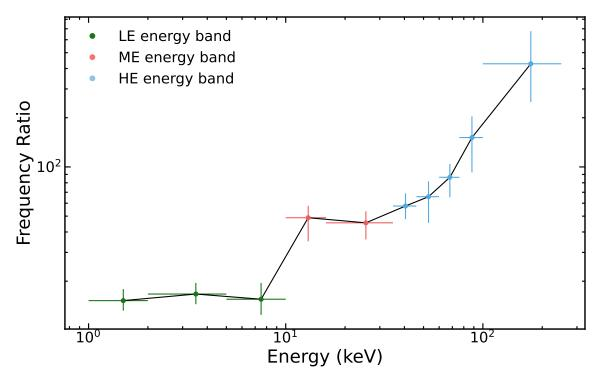


Figure 5. Ratio between the characteristic frequency of the L_h to that of the L_l components, indicating a significant broadening of the flat plateau of broadband noise in the PDS. Different colors represent data from different instruments.

the case of MAXI J1659-152 Yu & Zhang (2013)), the PLN seen below 2 keV could have been formed by such the two-way broadening of the characteristic frequency range, with L_l and L_h going below or beyond the frequency range of interest.

4.3. Conclusion

We have investigated the X-ray variability of MAXI J1820+070 in the hard state by modeling the PDS with three zero-centered Lorentzian components for the broad-band variability and a narrow Lorentzian component for the black hole low frequency QPO. We found the energy-dependent behaviors of the BLN power spectral components are in fact a two-way broadening phenomenon with increasing photon energy, i.e., the L_l component shifts towards lower frequencies while the L_h component shifts towards higher frequencies. The energy-dependent frequency broadening or separation of the BLNs produces an energy-dependent extension of the power plateau in the frequency domain with increasing photon energy, indicating that the seed photons which are up-scatted to higher energies (> 30 keV) originate from a wider range of the accretion disk. The energy-dependent trends of the two BLNs can be explained as due to the disk seed photons from different regions being up-scattered to the highest energies: one region corresponds to the very central inner disk embedded by the likely dense spherical corona and the other region corresponds to the disk region further out that is uncovered by the central corona; both regions of the accretion disk produce those seed photons up-scattered by the corona to the highest energies with the most number of up-scatterings. Interestingly, the trend of the two-way broadening of power spectrum would establish a power plateau in the PDS spanning over nearly two orders of magnitudes in frequency, mimic the emergence of the PLN seen in observations of MAXI J1659-152 when photon energies cross the boundary $\sim 2 \text{ keV}$, which shows that the PLN was also formed by a simultaneous broadening, flattening and amplitude-decreasing of the BLNs in the power spectra towards lower photon energies (see Figure 2 and 3 in Yu & Zhang (2013)). Such a simultaneous broadening in frequency, flattening of the power spectrum, and decreasing of fractional amplitude in the PDS might be a common process as the outcome of that the seed photons in Comptonization are from a wider, extended range in the thin disk flow.

ACKNOWLEDGEMENTS

We would like to thank Stefano Rappisarda, Wenda Zhang and Holger Stiele for helpful discussions. This work made use of the data from Insight-HXMT mission, a project funded by China National Space Administration (CNSA)

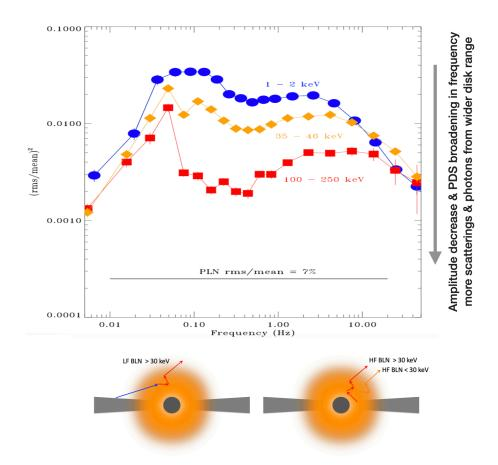


Figure 6. The schematic picture of the correspondence between the Comptonization geometries (lower) and the observed energy-dependent power spectra (upper panel) extracted in 1-2 keV (blue), 35-46 keV (orange), and 100-250 keV (red) from Obs-0601. The characteristic frequency of either the high frequency BLN component L_h or the low frequency BLN component L_l depends on the photon energy, which traces the radii at which the seed photons originate. A representative PLN with a fractional rms of 7% is shown as a horizontal solid line, indicating the PDS of BH soft state with approximately the maximal variability observed (Mao & Yu 2021).

and the Chinese Academy of Sciences (CAS). This work was supported in part by the Natural Science Foundation of China (grants U1838203, 12373050, and 12373049).

DATA AVAILABILITY

The Insight-HXMT data underlying this article are available in the public archive http://archive.hxmt.cn/proposal.

Facilities: HXMT

REFERENCES

Belloni, T., Psaltis, D., & Klis, M. v. d. 2002, The Astrophysical Journal, 572, 392, doi: 10.1086/340290
Belloni, T. M., & Motta, S. E. 2016, arXiv:1603.07872
[astro-ph], 440, 61, doi: 10.1007/978-3-662-52859-4_2

Buisson, D. J. K., Fabian, A. C., Barret, D., et al. 2019,
Monthly Notices of the Royal Astronomical Society, 490,
1350, doi: 10.1093/mnras/stz2681

- Done, C., Gierlinski, M., & Kubota, A. 2007, The Astronomy and Astrophysics Review, 15, 1, doi: 10.1007/s00159-007-0006-1
- Gao, C., Yan, Z., & Yu, W. 2023, Monthly Notices of the Royal Astronomical Society, doi: 10.1093/mnras/stad434
- Homan, J., Wijnands, R., Klis, M. v. d., et al. 2001, The Astrophysical Journal Supplement Series, 132, 377, doi: 10.1086/318954
- Ingram, A., & Done, C. 2011, MNRAS, 415, 2323, doi: 10.1111/j.1365-2966.2011.18860.x
- Ingram, A., & Done, C. 2011, Monthly Notices of the Royal Astronomical Society, 415, 2323. https://academic.oup. com/mnras/article-abstract/415/3/2323/1047536
- Kara, E., Steiner, J. F., Fabian, A. C., et al. 2019, Nature, 565, 198, doi: 10.1038/s41586-018-0803-x
- Kawamura, T., Axelsson, M., Done, C., & Takahashi, T. 2022, Monthly Notices of the Royal Astronomical Society, 511, 536, doi: 10.1093/mnras/stac045
- Kawamuro, T., Negoro, H., Yoneyama, T., et al. 2018, The Astronomer's Telegram, 11399, 1.
- https://ui.adsabs.harvard.edu/abs/2018ATel11399....1K
- Lyubarskii, Y. E. 1997, MNRAS, 292, 679, doi: 10.1093/mnras/292.3.679
- Lyubarskii, Y. E. 1997, Monthly Notices of the Royal Astronomical Society, 292, 679, doi: 10.1093/mnras/292.3.679
- Ma, X., Tao, L., Zhang, S.-N., et al. 2020, Nature Astronomy, doi: 10.1038/s41550-020-1192-2
- Mao, D.-M., & Yu, W.-F. 2021, Chinese Astronomy and Astrophysics, 21, 170, doi: 10.1088/1674-4527/21/7/170
- Méndez, M., van der Klis, M., Ford, E. C., Wijnands, R., & van Paradijs, J. 1999, ApJL, 511, L49, doi: 10.1086/311836
- Pozdnyakov, L. A., Sobol, I. M., & Syunyaev, R. A. 1983, Astrophysics and Space Physics Reviews, 2, 189. https://ui.adsabs.harvard.edu/abs/1983ASPRv...2..189P
- Remillard, R. A., & McClintock, J. E. 2006, Annual Review of Astronomy and Astrophysics, 44, 49,
 - doi: 10.1146/annurev.astro.44.051905.092532

- Shidatsu, M., Nakahira, S., Murata, K. L., et al. 2019, The Astrophysical Journal, 874, 183, doi: 10.3847/1538-4357/ab09ff
- Shidatsu, M., Nakahira, S., Yamada, S., et al. 2018, The Astrophysical Journal, 868, 54, doi: 10.3847/1538-4357/aae929
- Stiele, H., & Yu, W. 2014, Monthly Notices of the Royal Astronomical Society, 441, 1177, doi: 10.1093/mnras/stu646
- —. 2015, Monthly Notices of the Royal Astronomical Society, 452, 3666, doi: 10.1093/mnras/stv1530
- Tananbaum, H., Gursky, H., Kellogg, E., Giacconi, R., & Jones, C. 1972, ApJL, 177, L5, doi: 10.1086/181042
- Tucker, M. A., Shappee, B. J., Holoien, T. W.-S., et al. 2018, The Astrophysical Journal Letters, 867, L9, doi: 10.3847/2041-8213/aae88a
- Van der Klis, M. 2006, csxs, 39, 39
- Wijnands, R., & Klis, M. v. d. 1999, The Astrophysical Journal, 514, 939, doi: 10.1086/306993
- Yang, Z.-X., Zhang, L., Bu, Q.-C., et al. 2022, ApJ, 932, 7, doi: 10.3847/1538-4357/ac63af
- Yang, Z.-X., Zhang, L., Bu, Q.-C., et al. 2022, The Astrophysical Journal, 932, 7, doi: 10.3847/1538-4357/ac63af
- Yu, W., Klein-Wolt, M., Fender, R., & Klis, M. v. d. 2003, The Astrophysical Journal, 589, L33, doi: 10.1086/375714
- Yu, W., & Zhang, W. 2013, The Astrophysical Journal, 770, 135, doi: 10.1088/0004-637X/770/2/135
- Yu, W., Zhang, S. N., Harmon, B. A., et al. 1997, ApJL, 490, L153, doi: 10.1086/311033
- Zhang, S.-N., Li, T., Lu, F., et al. 2020, Science China Physics, Mechanics & Astronomy, 63, 249502, doi: 10.1007/s11433-019-1432-6